AN ABSTRACT OF THE THESIS OF

Frederick L. Bahr for the degree of Master of Science in

Oceanography presented on July 19, 1991 .

Title: The Effects of Rainfall on Temperature and Salinity in the Surface Layer of the Equatorial Pacific

Abstract approved: Redacted for privacy

Clayton A. Paulson

Measurements of temperature and salinity in the upper 5 m of the ocean along the equator showed cool fresh anomalies due to rain showers. The measurements were made between 140 W and 110 W during April 1987, an El Nino year. The eastern equatorial Pacific was characterized by weak winds (3 m/s average), high rainfall (1.6 cm/day), and warm surface temperatures (28.4 C). Measurements of temperature were made from a catamaran float at 0.5 and 1 m depth and at 5 m depth from the ship. Salinity was measured at a depth of 1 m from the float and 5 m from the ship. The float was towed off of the port side of the ship outside of the bow wake. Near-surface low temperature and low salinity anomalies due to cool rainfall were encountered. These anomalies were on average cool and fresh by 0.02 C and 0.2 PSU with maximum values of 0.5 C and 1.6 PSU. The horizontal extent of the anomalies ranged from less than 10 to more than 100 km. Rainfall depths estimated from salt conservation agreed roughly with shipboard rain-gauge measurements. The characteristic lifetime of the anomalies, estimated from the ratio of the average rain depth to average rain rate, was about 10 hrs.

Rainfall temperatures were computed from the T-S mixing curves for three large, newly-formed anomalies. The average rainfall temperature was 21 C. Ocean buoyancy fluxes estimated for intense rain showers were an order of magnitude larger than the fluxes in the absence of rain.

The Effects of Rainfall on Temperature and Salinity in the Surface Layer of the Equatorial Pacific

by

Frederick L. Bahr

A THESIS

submitted to

Oregon State University

in partial fulfillment of

the requirements for the

degree of

Master of Science

Completed July 19, 1991

Commencement June 1992

APPROVED:

Redacted for privacy

Professor of Oceanography in charge of major

Redacted for privacy

Dean of College of Oceanography

Redacted for privacy

Dean of Graduate School

Date thesis is presented July 19, 1991

Typed by Frederick L. Bahr

TABLE OF CONTENTS

LIST OF FIGURES

The smooth curve was adjusted to have the same mean as the data. Diurnal heating is evident in the temperatures. Rainfall events appear as fresh anomalies in the salinity relative to the smooth curve. Several of the rainfall events have cool temperature anomalies associated with them (Days 105, 110, and 117). Days are labeled at 0 GMT on this and subsequent plots. 11

3. Salinity in the upper 31 m for the zonal transect along the equator from 140 W to 110 W contoured in depth vs time/space, with a five-shade gray scale that rolls over at 1.0 PSU. In the vertical, the data are at 1 m and every odd meter below 5 m. The data has been averaged to 3 hrs. The freshest water was located near the surface at 110 W. 15

4. Salinity in the upper 31 m for the meridional transect along 110 W from 3 S to 6 N where the data have been averaged to 1 hr. The same gray scale is used as in Fig. 3. The freshest water was located near the surface between 3 N and 4 N. 16

5. Temperature-salinity (T-S) diagram of the 30-s samples at 1-m depth for the zonal transect along the equator. The slanted solid lines are lines of constant σ_t and are plotted at 0.5 kg m^{-3} increments. 17

6. Time/space series of hourly averages of meteorological measurements from the *Wecoma* and the total heat flux (positive upward) from April 15 (Day 105) to April 28 (Day 118) along the equator from 140 W to 110 W. Incoming short-wave radiation (SW), air temperature, and humidity were measured at a height of 8 m. Wind speed was measured on the mast at a height of 20 m. 19

7. Distances across anomalies are plotted against average magnitude of the salinity anomalies. The magnitude of the anomalies are defined as the average difference between the 1-m salinity and the smooth curve value. Each mean must contain 12 points (corresponding to 6 min of data). Anomalies were computed from the 30-s samples. 22

8. Time/space series of 30-s, 1-m salinities and hourly standard deviations of the 1-hr mean salinities. The smooth curve is the same as in Fig. 2. 24

9. The anomaly on Day 105 showing time/space series of 60-s wind speed, 30-min wind direction and 30-s air temperature, density, temperature, and salinity data. The depths corresponding to different lines are defined in Fig. 2 (*e.g.* 0.5 m (thin line), 1 m (dashed line), 5 m (thick line)). The arrows mark the start and stop times of the 30-s, 1-m temperature and salinity data used to compute the rainfall temperature. 27

LIST OF TABLES

3. Characteristics of selected rainfall anomalies including start time, duration (Δt), vertical temperature gradient (ΔT), salinity anomaly (ΔS), rainfall temperature (Rain T) and 80% confidence interval of rainfall temperatures. All anomalies were selected which met the following criteria: $\Delta t > 35$ minutes, $\Delta S < -0.6$ PSU and $\Delta T < -0.1$ C. ΔS is the minimum difference (maximum absolute difference) between the smoothed background salinity and the 1-m salinity and ΔT is the minimum difference (maximum absolute difference) between the 0.5-m temperature and the 5-m temperature. The 80% confidence intervals for the individual estimates were computed following Bendat and Piersol (1986, Eq. 4.75, page 104). The 80% confidence interval for the average rainfall temperature was computed following Bendat and Piersol (1986, Eq. 4.46, page 86).

The Effects of Rainfall on Temperature and Salinity in the Surface Layer of the Equatorial Pacific

Introduction

The climatology of surface salinity in the open ocean is highly correlated with the air-sea flux of fresh water (see *e.g.* Pickard and Emery, 1982). In the long-term averages, there are zonal bands of high and low salinity which correspond to positive and negative values of evaporation minus precipitation. Despite the influence of rainfall on the large-scale climatology of the upper ocean, there have been relatively few field measurements of the short-term, small-scale effects of rain on the surface layer. This paper focuses on an analysis of rain-caused salinity and temperature anomalies in the surface layer of the eastern equatorial Pacific.

Ostapoff *et. al.* (1973) analyzed 18 hrs of data from the tropical Atlantic and made estimates of rainfall from the change in salinity. They also described the effects of rain on decreasing the depth of the oceanic mixed layer.

Price (1979) described the evolution of a rain-formed mixed layer off the west Florida coast. An estimated 6 cm of rain fell over less than 2 hr, approximating an impulsive buoyancy flux. The salinity anomaly then evolved with depth in response to surface forcing.

Ginzburg *et. al.* (1980) made towed observations during heavy rain showers in the western Sargasso Sea in which they measured salinity anomalies of 0.5–1.0 PSU and cool-temperature anomalies of 0.2 C in the upper 1 m. Also observed, were what they called "fossil rain" signatures. These were fresh lenses which were cool at night and warm during the day, presum-

ably caused by the diurnal cycle of heating and cooling of a salt-stratified layer.

Volkov *et. al.* (1989) measured temperature and salinity fluctuations in the upper 2 m of the Atlantic ocean between 2 N and 7 N by use of instruments mounted on the bow of a ship. Traces of freshening caused by rainfall were associated with warm anomalies caused by enhanced solar heating of the salt-stratified lenses.

Lukas (1990) reported shipborne thermosalinograph measurements at 4-m depth which show rain-caused temperature/salinity anomalies in the western equatorial Pacific. The distance across one of these anomalies was 20 km and the temperature and salinity depressions were approximately 0.3 C and 0.5 PSU respectively. Temperature-salinity (T-S) plots of 10 days of thermosalinograph data from the same cruise show many cold, fresh anomalies caused by rain from convective cells.

This paper presents the results of an analysis of underway, shipborne measurements of temperature and salinity made in the upper 5 m along the equator in the eastern Pacific. The measurements show cold, fresh anomalies caused by rain. The measurements were made in April, 1987, during the 1986–87 *El Niño*, characterized by warmer than average surface temperatures, below average wind speeds and higher than average rainfall in the eastern equatorial Pacific. The objectives of this paper are: 1) to describe the characteristics of rain-caused anomalies 2) to estimate rainfall amounts and temperatures, 3) to describe the evolution of rain-caused anomalies and 4) to estimate the effects of rainfall on air-sea exchanges.

Instruments

The upper 5 m of the ocean was sampled by temperature and conductivity sensors installed on a small catamaran and on the R/V *Wecoma*. The catamaran (Fig. 1) was towed 8 m off of the port side of the ship to avoid the bow wake. The catamaran had a conductivity sensor at a depth of 1 m and temperature sensors at depths of both 1 and 0.5 m. Temperature at 5-m depth was measured with thermistors in the sea chest and in the transducer well of the ship (Fig. 1). Both locations are near the ship's keel. Salinity measurements at 5 m were from water pumped from the sea chest to the ship's lab where temperature and conductivity were sampled continuously and samples of water were taken every two hours and analyzed for salinity. All of the temperature and conductivity sensors were sampled at 30-s intervals. A list of the instruments and their characteristics is given in Table 1.

The 5-m, 30-s salinity measurements were corrected for drift due to sensor fouling by comparison with salinity from water samples (bottles) taken every 2 hrs. Differences were computed between bottle salinities and the nearest (in time) 30-s salinity sample. A linear least squares fit vs time was computed for the differences and used to correct the 5-m data. The root mean square (rms) difference between the fit and the data was 0.006 PSU.

The 1-m salinities were corrected by use of the 5-m salinities. Half-hour sequential means were computed for both salinities. When the upper 5 m of the ocean was considered to be homogeneous, differences were computed. The differences were computed only if the following criteria for homogeneity were met: wind speed greater than 3 m/s, standard deviation of the wind speed less than 0.5 m/s, standard deviation of both salinities less then 0.05 PSU, means computed from at least 50% of the total possible number

Fig. 1. Side views of the R/V *Wecoma* and the catamaran float. The float was towed approximately 8 m off of the port side of the ship. Wind speed was measured at a height of 20 m from the mast of the ship. The other meteorological instruments were located at a height of 8 m. Temperature was measured at depths of 0.5 and 1 m from the float and 5 m from the ship. Salinity was measured at depths of 1 m from the float and 5 m from the ship.

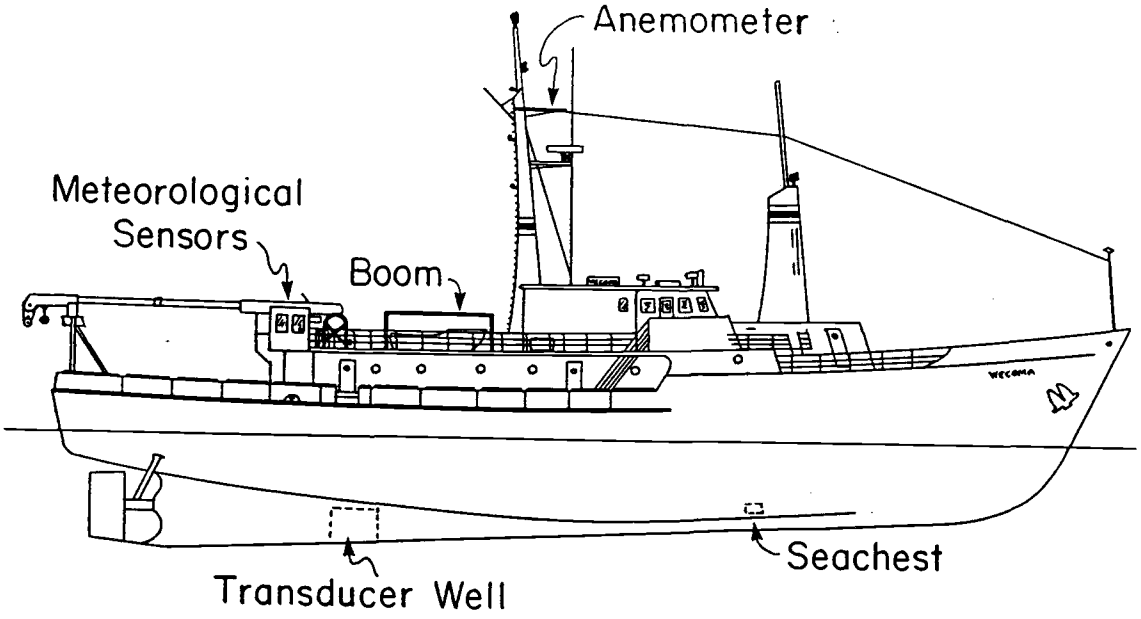
Anemometer
Meteorological
Sensors
Boom
Seachest
Transducer Well

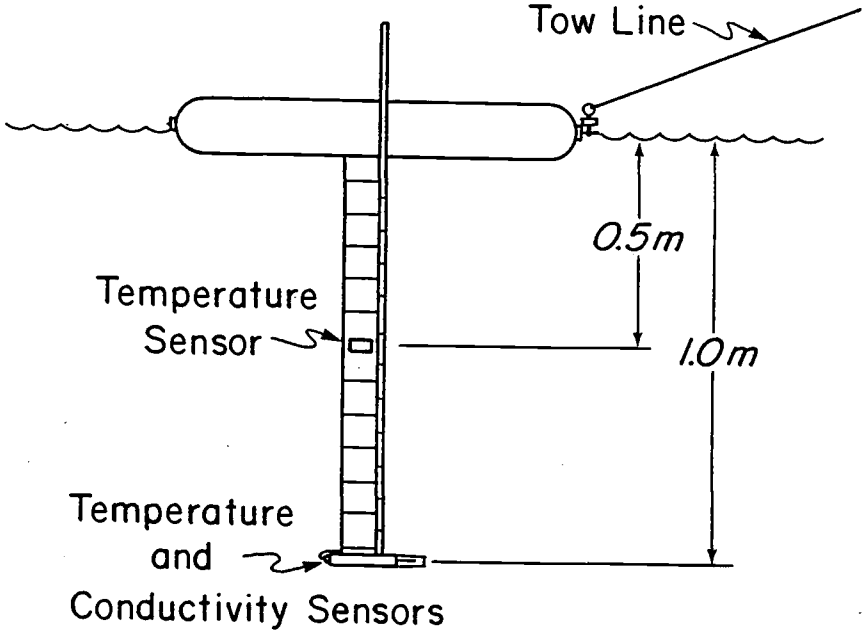
Tow Line
0.5m
Temperature
Sensor
1.0m
Temperature
and
Conductivity Sensors

Fig. 1.

Table 1. Characteristics of instruments used including manufacturer, model, accuracy, and response along with the elevation of the instrument above the sea surface.

Table 1.

Measurement	Manufacturer/model	Accuracy	Response	Elevation
Long-wave radiation	Eppley Laboratory model PIR	±1.0% full scale	2.0 s	8.6 m
Short-wave radiation	Eppley Laboratory model 8–48	±1.0% full scale	3–4 s	8.6 m
Relative humidity	Rotronic Instr. model MP–100	1.5%	< 10 s	7.5 m
Air temp.	Yellow Springs Instr. model 44003	0.2 C	60 s	8.4 m
Wind speed and dir. (2 sensors)	Belfort Instr. model 5–120	1.0% 3 deg	4.6 m 10.7 m	20 m 20 m
Temperature (catamaran)	Thermometrics model P–85	0.01 C	0.1 s	−0.5 m
Conductivity (catamaran)	Sea-Bird Electronics model SBE–4	0.001 mho m^{-1}	0.2 s	−1.0 m
Temperature (catamaran)	Sea-Bird Electronics model SBE–3	0.01 C	0.2 s	−1.0 m
Temperature (ADCP head)	RD Instr./Yellow Springs Instr. model RD-VM ADCP	0.1 C	140 s	−5.0 m
Temperature (sea chest)	Aanderaa/Fenwal Electronics model GB–32JM19	0.1 C	12 s	−5.0 m
Conductivity (water pumped to lab from sea chest)	Sea-Bird Electronics model SBE–4	0.001 mho m^{-1}	0.2 s	−5.0 m
Temperature (water pumped to lab from sea chest)	Sea-Bird Electronics model SBE–3	0.01 C	0.2 s	−5.0 m

of points and also, differences were only computed during the night time between 7:24 pm and 6:12 am local time. This time interval was chosen to take account of the 2-hr shift in sunset and sunrise times between 110 W and 140 W. The variance of the wind speed was used to obtain periods when the wind speed was relatively constant. The variance of the salinity was used to objectively eliminate points which may have been influenced by rainfall. The number-of-points criteria was used to obtain a representative mean. A least squares linear fit to the differences vs time was computed and applied to the 1-m data. The rms difference between the fit and the data was 0.001 PSU.

The 0.5-m temperature was corrected for small shifts of approximately 0.01 C. Ten-minute sequential means were computed from the 30-s differences between the 0.5 and 1-m temperatures. Means were compared only if they satisfied the above criteria used for comparing the salinities except the standard deviation of the difference had to be less than 0.05 C. Linear least squares fits vs time were computed for three time intervals and applied to the 0.5-m data. The rms differences of the fits were 0.001, 0.002 and 0.001 C respectively.

No corrections were applied to the 1 and 5-m temperatures. Sequential half-hour means were computed for the 0.5, 1 and 5-m temperatures. Means were compared only if they satisfied the criteria given above. The mean difference between the 1 and 5-m sensors was -0.0025 C with an rms value of 0.01 C. The rms differences with respect to the mean between the 0.5 and 5-m and the 0.5 and 1-m sensors were 0.01 C and 0.004 C respectively. After the corrections, the temperatures had a relative accuracy in the upper 4.5 m of 0.01 C. The salinities, with the corrections, had a relative accuracy

of 0.001 PSU over 4 m.

Meteorological instruments were installed on the ship's mast and on top of the winch control station on the starboard side of the ship (Fig. 1). Wind speed and direction were measured with propeller/vane anemometers on both sides of the mast at a height of 20 m above sea level. Air temperature, relative humidity, incoming solar radiation and incoming long-wave radiation were measured at a height of 8 m on top of the winch control station (Fig. 1). Air temperature was sampled at 30-s intervals and all other variables were sampled once every 60 s. A rain gauge was also mounted on top of the winch control station at a height of 8 m. The instruments and their characteristics are listed in Table 1. Because of the large uncertainty in rain-gauge measurements due to factors unrelated to the instrument, the characteristics of the Taylor Clear-Vu rain gauge, model 2701, were left out of Table 1. Standard shipboard meteorological observations were taken both by the ship's crew and the scientific crew at 2-hr intervals. These data were used to check the automated meteorological measurements. Additionally, visual observations of rainfall by the ship's crew were used with the rain-gauge observations in the identification of newly-formed anomalies.

Observations

A variety of underway observations were taken aboard the R/V *Wecoma* in the equatorial eastern Pacific during April and May 1987. Two transects were made, the first from 140 W to 110 W (April 15–28) along the equator, and the second from 3 S to 6 N (May 1–5) along the 110 W meridian. The average speed of the ship during these transects was 2.8 m/s. The primary focus of this paper is on the temperature and salinity measurements made in the upper 5 m. Meteorological observations were also made and are valuable aids in the interpretation of the oceanic data. Measurements of temperature and salinity below 5-m depth were taken with a microstructure profiler (Hebert *et. al.*, 1991). These observations are used here to extend the description of salinity anomalies down to a depth of 30 m.

Time/space series of the hourly averaged temperature and salinity measurements taken along the equator from 140 W to 110 W are shown in Fig. 2. Low salinity anomalies, caused by rain, were common. Salinities measured at 1 and 5-m depths were nearly indistinguishable, *i.e.* the magnitude of the anomalies was large compared to the difference in salinity between 1 and 5 m. Some of the low-salinity anomalies were anomalously cold, *e.g.* on Days 105 and 117, where the 0.5-m temperature record was colder than the deeper measurements. There were also diurnal variations in the temperature, caused by solar heating, with maximum excursions at 0.5-m depth.

Surface temperature and salinity along the transect from 140 W to 110 W can be compared to the Levitus (1982) climatology. Mean and extreme values of hourly averaged near-surface temperature and salinity are shown in Table 2. The mean surface temperature was much warmer, 28.4 C, than the climatological winter (February, March, April) mean of 25.7 C

Fig. 2. Time/space series of sequential hourly averages of near-surface temperature, salinity, and rainfall. Temperatures were measured at depths 0.5 m (thin line), 1 m (dashed line) and 5 m (thick line). Salinities were measured at depths of 1 m (dashed line) and 5 m (thick line). A smooth curve was fitted to the 1 m salinity data (as described in the text) and is shown with a thick line. Rain-gauge measurements (octagons) and rainfall computed from salinity anomalies (line) are shown in the bottom panel. Observations of rainfall (steady precipitation) on the ship's bridge are denoted with downward pointing triangles and showers (short intense periods of precipitation) are denoted with upward pointing triangles.

The smooth curve was adjusted to have the same mean as the data. Diurnal heating is evident in the temperatures. Rainfall events appear as fresh anomalies in the salinity relative to the smooth curve. Several of the rainfall events have cool temperature anomalies associated with them (Days 105, 110 and 117). Days are labeled at 0 GMT on this and subsequent plots.

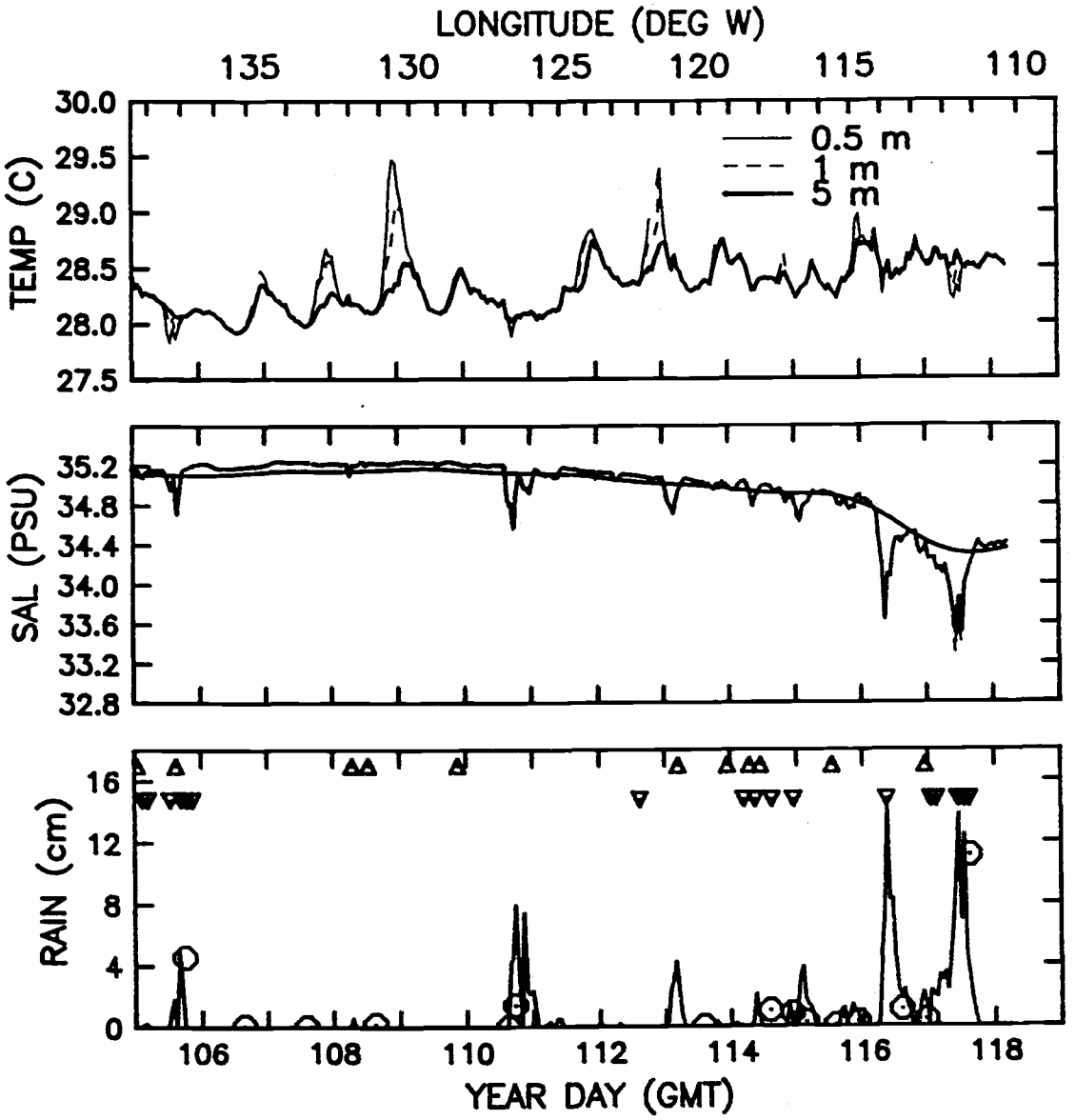
LONGITUDE (DEG W)
135
130
125
120
115
110
TEMP (C)
30.0
29.5
29.0
28.5
28.0
27.5
0.5 m
1 m
5 m
SAL (PSU)
35.2
34.8
34.4
34.0
33.6
33.2
32.8
RAIN (cm)
16
12
8
4
0
106
108
110
112
114
116
118
YEAR DAY (GMT)

Fig. 2.

Table 2. Mean, minimum and maximum values of measured and estimated variables along the equatorial transect. The values were computed from sequential hourly means except for rain rate. The mean rain rate is the sum of shipboard rain-gauge measurements divided by the length of time of the transect. The maximum rain rate was determined from sequential readings of the rain gauge divided by the time between readings (maximum was 11 cm over 15 hr). The wind speed and stress means are averages of magnitudes (not vector averages). The buoyancy and net heat fluxes do not include the effect of rain. A positive heat flux corresponds to a cooling of the ocean and a positive buoyancy flux to a stabilization of the surface layer. The numbers in parentheses exclude Days 116–118, a period which had exceptionally high values of rainfall measured by a rain gauge and estimated from the salinity anomaly.

Variable	Mean	Min	Max	Units
T at 0.5 m	28.37	27.83	29.47	C
T at 1 m	28.36	27.91	29.28	C
T at 5 m	28.33	27.92	28.83	C
S at 1 m	34.96	33.30	35.25	PSU
S at 5 m	34.96	33.47	35.25	PSU
Wind Speed	3.2	0.4	9.3	m/s
Air Temp	27.1	23.4	29.5	C
Rel Humid	82.2	70.3	99.4	%
Wet Bulb T	24.7	22.6	26.1	C
Rain (S Anom)	0.72 (0.32)	0	14.2 (8.0)	cm
Rain Rate	1.6 (0.8)	0	17.2	cm/day
Rain Rate	19 (9)	0	200	10^{-5}kg m^{-2}s^{-1}
Evaporation	2.6	0.5	7.9	10^{-5}kg m^{-2}s^{-1}
Stress	0.019	0	0.12	N/m^2
Net Heat Flux	−94	−830	230	W/m^2
Rain Heat Flux	6 (3)	0	61	W/m^2
Buoyancy Flux	6.8	−21	67	10^{-6}kg m^{-2}s^{-1}
Rain Buoy. Flux	4.6 (2.2)	0	48	10^{-6}kg m^{-2}s^{-1}

(Levitus, 1982). The value was about 1 C warmer than the climatological April value of 27.5 C (Esbensen and Kushnir, 1981). The warm surface value compared to climatology is consistent with the warming which occurs during an *El Niño* in the eastern Pacific (Philander, 1990). The mean salinity, 34.96 PSU, however was very close to the climatological winter value of 34.89 PSU (Levitus, 1982).

Vertical distributions of salinity, down to a depth of 30 m, along both transects are shown in Figs. 3 and 4. Figures 3 and 4 were constructed using the 1 and 5-m data along with data from a microstructure profiler whose shallowest reliable measurement is 10 m (Hebert *et. al.*, 1991). Comparing Fig. 3 and Fig. 2, it can be seen that most anomalies did not extend below 5 m (the anomalies in Fig. 2 appear in Fig. 3 as fresh blobs at 1 and 5 m). The anomalies on Days 116 and 117 were the only ones which appeared to penetrate as deep as 30 m. In the meridional section, Fig. 4, a large fresh pool was located at approximately 3.5 N. The large fresh pool was probably caused by rainfall from several convective systems. The location of the fresh pool was coincident with the seasonal excursion of the intertropical convergence zone (ITCZ). The ITCZ moves seasonally from its southern most position, near the equator in March and April, to approximately 12 N, in August and September (Philander, 1990). The surface value of the salinity on the equator at 110 W at the end of the zonal transect was 34.4–34.6 PSU. The surface value 3 days later was 34.8–35.0 PSU. Water with the same salinity as the zonal transect was now located at 0.6 N. If the water was simply advected north it would require a speed of 0.3 m/s. The change in salinity could also have been affected by mixing with the surrounding water.

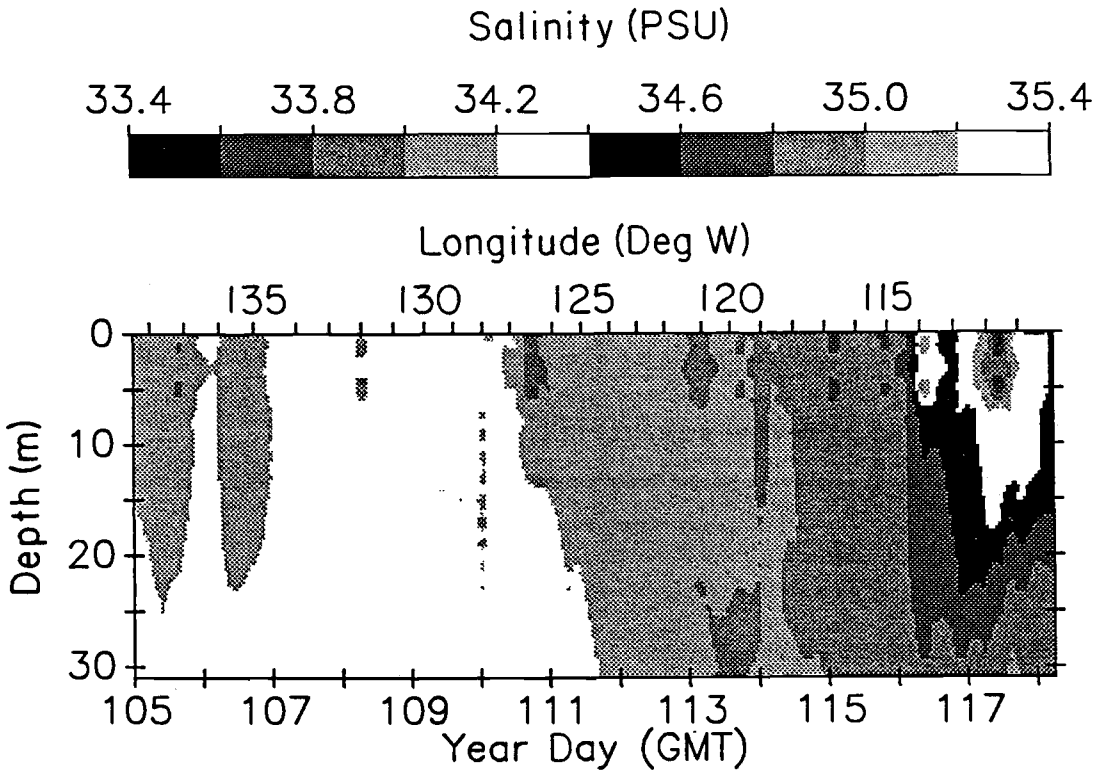

Fig. 3. Salinity in the upper 31 m for the zonal transect along the equator from 140 W to 110 W contoured in depth vs time/space, with a five-shade gray scale that rolls over at 1.0 PSU. In the vertical, the data are at 1 m and every odd meter below 5 m. The data have been averaged to 3 hrs. The freshest water was located near the surface at 110 W.

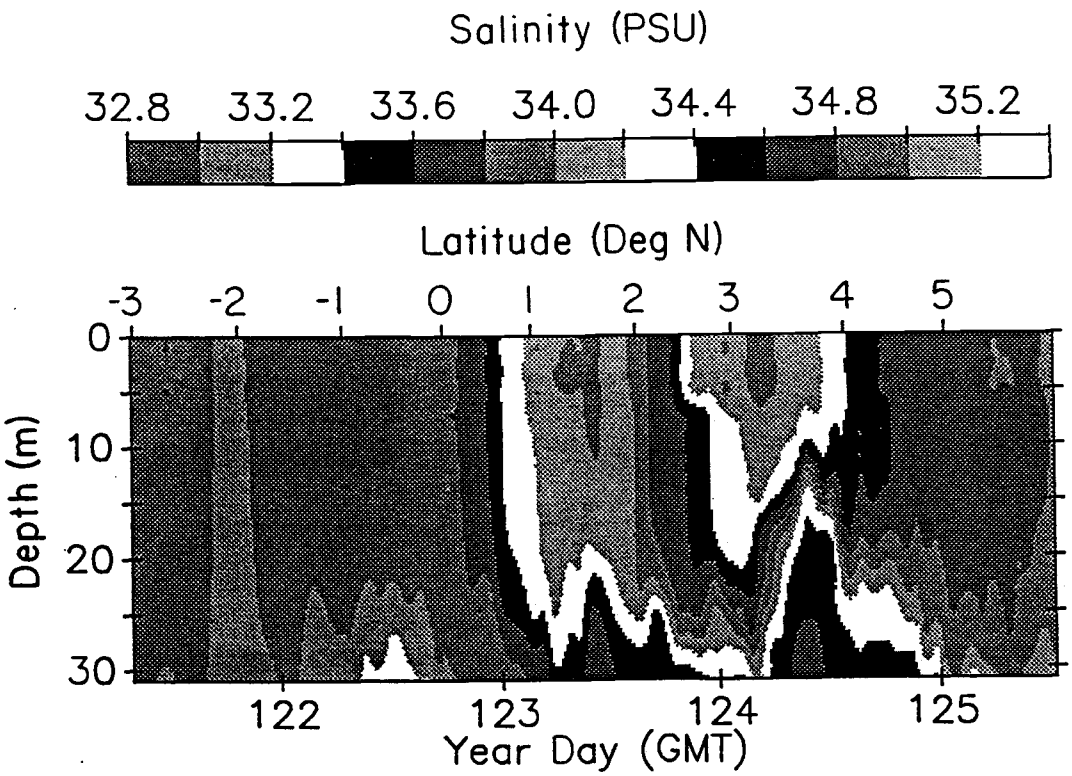

Fig. 4. Salinity in the upper 31 m for the meridional transect along 110 W from 3 S to 6 N where the data have been averaged to 1 hr. The same gray scale is used as in Fig. 3. The freshest water was located near the surface between 3 N and 4 N.

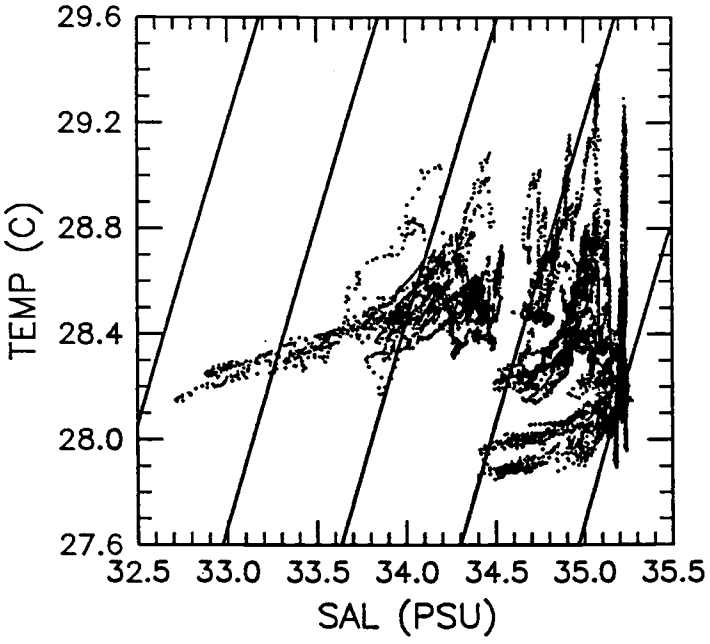

Fig. 5. Temperature-salinity (T-S) diagram of the 30-s samples at 1-m depth for the zonal transect along the equator. The slanted solid lines are lines of constant σ_t and are plotted at 0.5 kg m^{-3} increments.

The 30-s samples at 1-m depth of temperature and salinity from the entire zonal transect are plotted as T vs S in Fig. 5. Rainfall anomalies appear as lines of points extending towards low salinity and temperature. Also apparent are diurnal variations of temperature which appear as vertical lines of points, seen most clearly, on the right side of the figure.

Meteorological measurements were taken throughout the zonal transect. Selected measurements along with the computed total heat flux (excluding the heat flux associated with rainfall) are shown in Fig. 6. Rain gauge measurements and bridge observations of rain are plotted in the lower panel of Fig. 2. Mean and extreme values of many of the meteorological measurements and the derived air-sea fluxes are given in Table 2. Fluxes were computed following Large and Pond (1981; 1982).

Meteorological conditions during the zonal transect were marked by low mean wind speed, occasional squalls and higher than normal rainfall (Table 2). The mean wind speed over the zonal transect was 3.2 m/s compared to the long-term annual mean of 6 m/s (Weare *et. al.*, 1981). The squalls (Days 110 and 117, *e.g.*) had peak winds as high as 9 m/s, cool air temperatures and rain. The average rainfall during the zonal transect was 1.6 cm/day compared to a climatological annual average of 0.14 cm/day (Taylor, 1973). If Days 116-118 are excluded, the mean drops to 0.8 cm/day. The latent heat flux, 63 Wm^{-2}, was 2/3 of the climatological value for April of 100 Wm^{-2} (Esbensen and Kushnir, 1981). The net long-wave heat flux, 27 Wm^{-2}, was approximately 50% of the climatological April value, 55 Wm^{-2} (Esbensen and Kushnir, 1981).

Fig. 6. Time/space series of hourly averages of meteorological measurements from the *Wecoma* and the total heat flux (positive upward) from April 15 (Day 105) to April 28 (Day 118) along the equator from 140 W to 110 W. Incoming short-wave radiation (SW), air temperature, and humidity were measured at a height of 8 m. Wind speed was measured on the mast at a height of 20 m.

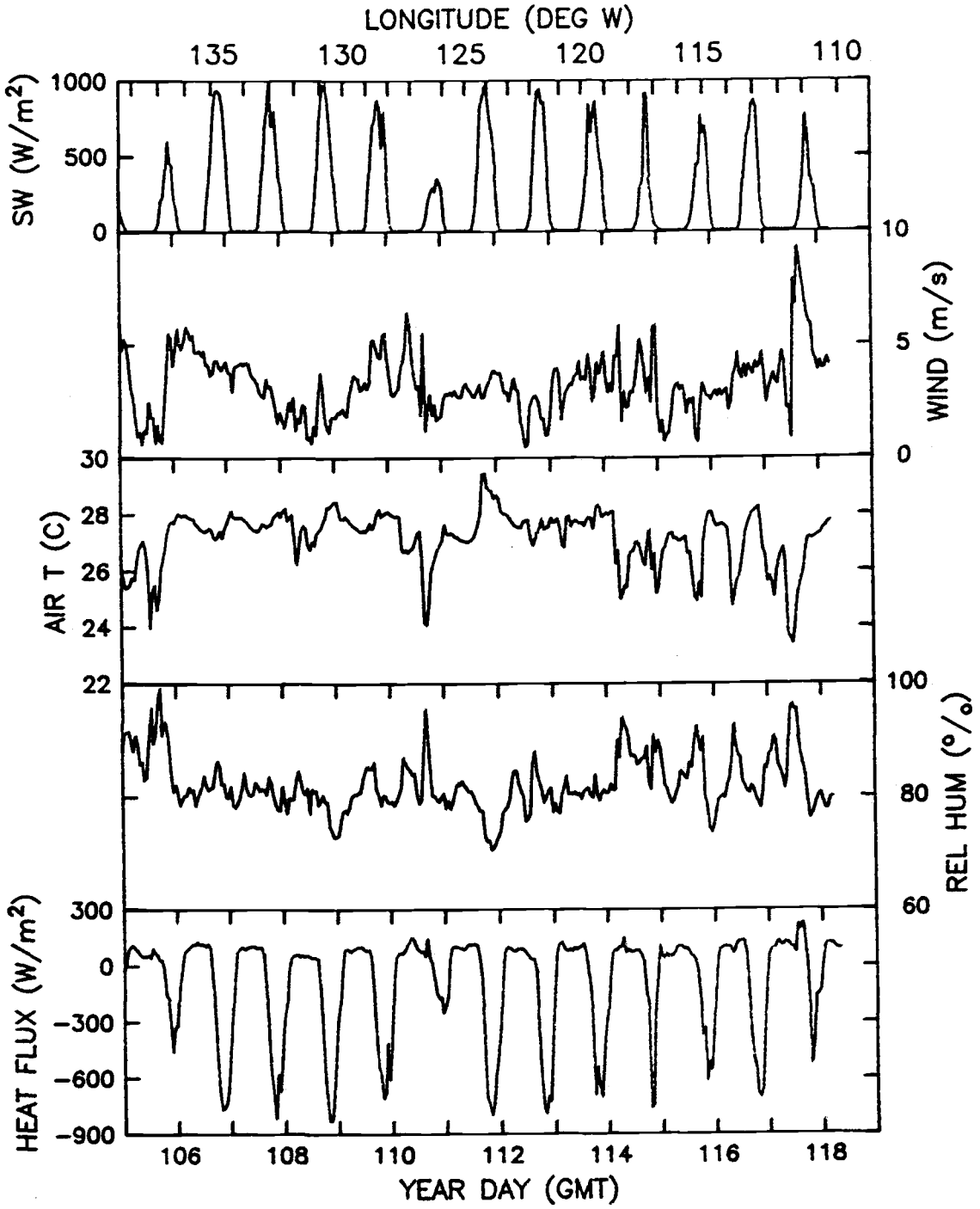
LONGITUDE (DEG W)
135
130
125
120
115
110
SW (W/m²)
1000
500
0
10
WIND (m/s)
5
0
30
AIR T (C)
28
26
24
22
100
REL HUM (%)
80
60
300
HEAT FLUX (W/m²)
0
-300
-600
-900
106
108
110
112
114
116
118
YEAR DAY (GMT)

Fig. 6.

Rain-caused T-S anomalies

Rain-caused salinity anomalies are defined as intervals of time/space where the observed 1-m salinity was less than the smoothed salinity. Measured and smoothed salinity are shown in the middle panel of Fig. 2. In determining the smooth curve, it was assumed that maximum values of salinity are representative of background values, undisturbed by recent rainfall. For Days 114–118, the observed general decrease in salinity was considered to be the background salinity to the smaller scale anomalies located within this time period. The smoothed salinity was determined from the maximum hourly average values of 1-m salinity observed during sequential 12-hr periods. These maxima were linearly interpolated onto a 12-hr grid, a linear trend connecting the end points was subtracted, and a 9-term periodic Fourier expansion computed. A 9-term Fourier series was used because it reproduced the large scale features of the measured salinity qualitatively. The resulting smoothed salinity was adjusted vertically so that its mean over the transect was equal to the mean of the 1-m data. Other methods to obtain a smooth curve, such as a running mean or a polynomial fit, gave unsatisfactory results.

As discussed above, most anomalies do not appear to penetrate deeper than 5 m. Figure 3 indicates that only the anomaly on Days 116 and 117 extended deeper than 10 m, to a depth of 30 m.

The horizontal extent of anomalies ranged from less than 1 km to over 100 km. The horizontal extent of the anomalies was computed from records of the ship's position. A plot of the magnitude of rain-caused salinity anomalies vs the distance across the anomalies is shown in Fig. 7. The magnitude of an anomaly is the average difference between the smoothed salinity and the

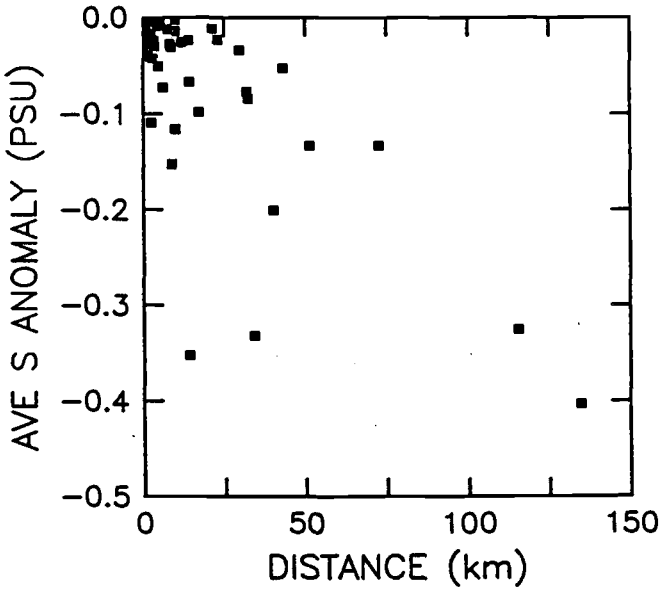

Fig. 7. Distances across anomalies are plotted against average magnitude of the salinity anomalies. The magnitude of the anomalies are defined as the average difference between the 1-m salinity and the smooth curve value. Each mean must contain 12 points (corresponding to 6 min of data). Anomalies were computed from the 30-s samples.

30-s samples within the anomaly. The boundaries of an anomaly are defined when the 30-s samples of salinity at 1-m depth are less than the smoothed salinity. Anomalies with fewer than 12 points (less than 6 min in duration or 1 km in extent) were excluded. A total of 45 anomalies are plotted. It should be noted that the estimates of horizontal extent will tend to be biased toward values which are too small because the sampling line is random, not necessarily across the maximum dimension of an anomaly.

The amplitude of small-scale fluctuations of salinity and temperature within the anomalies was much larger than in the surrounding fluid as is shown in Fig. 8 for salinity. The hourly rms deviations from the mean show that the anomalies have an order of magnitude higher variability than their surroundings.

Rainfall was estimated from the salinity anomalies by use of conservation of salt. For an anomaly with average salinity, S_a, extending from the surface to depth d_a, the estimated depth of the rainfall, d_r, which caused the anomaly is

$$d_r = d_a \frac{S_i - S_a}{S_i}$$

where S_i is the "initial" or average salinity in a surface layer of depth d_a before the rainfall, and is assumed to be the smoothed salinity (Fig. 2). In obtaining the estimates shown in Fig. 2, d_a was assumed to be 5 m and a constant vertical gradient based on the observations at 5 and 1 m was also assumed. S_a is the average salinity in the 5-m layer.

Rainfall may be underestimated by assuming that the anomaly is limited to 5-m depth. Figure 2 shows that there were usually small gradients in salinity between depths of 1 and 5 m, suggesting that the estimates of rainfall may be systematically too small. The salinity measurements shown in Fig. 3

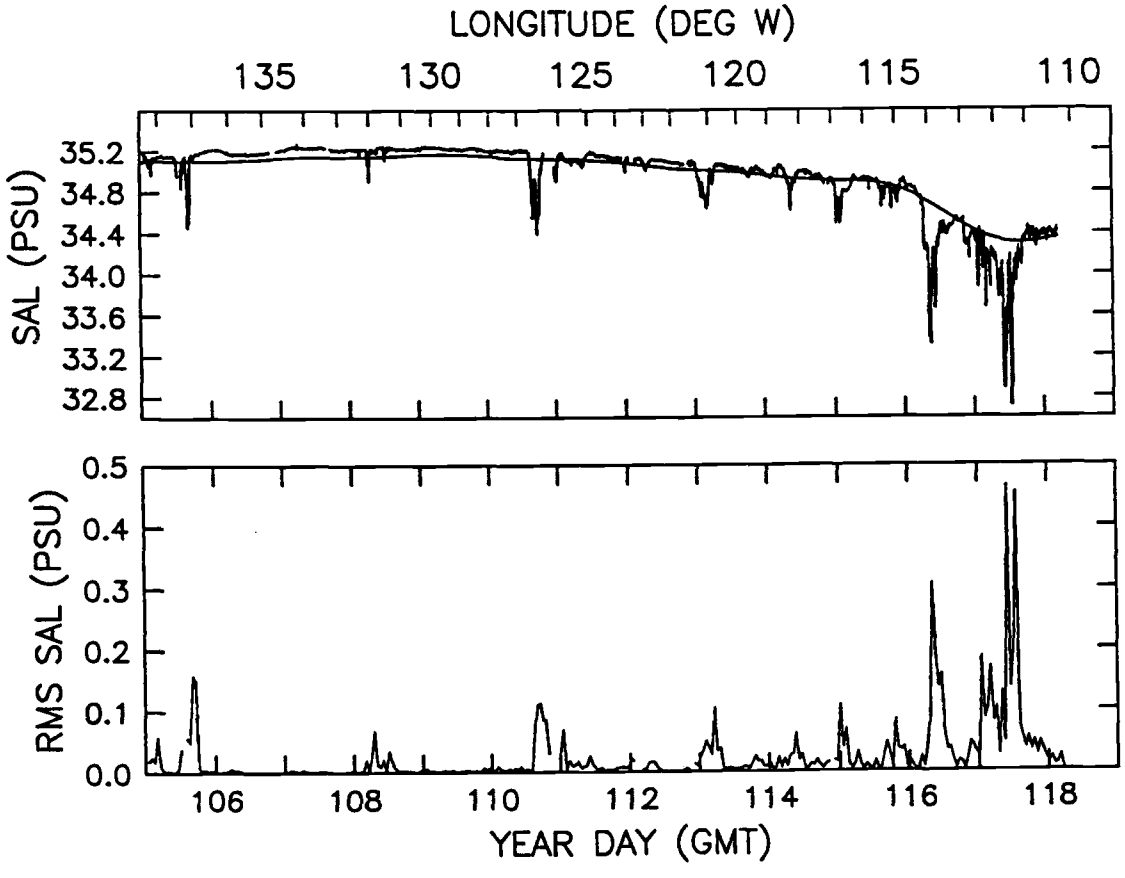

Fig. 8. Time/space series of 30-s, 1-m salinities and sequential hourly standard deviations of the 1-hr mean salinities. The smooth curve is the same as in Fig. 2.

indicate that the anomalies did not usually penetrate to 10-m depth, with the notable exception of the large anomalies on Days 116 and 117 which extended to a depth of 30 m.

The maximum values of rainfall estimated from the salinity anomalies agree well with the maximum rain-gauge measurement (Fig. 2 and Table 2). The maximum rain-gauge measurement was 11 cm over 15 hr and was close to a local maximum of 14 cm of rain estimated from the salinity anomaly (Day 117).

The characteristic time scale or lifetime of the rain-caused salinity anomalies can be estimated from the ratio of the average depth of rain estimated from the anomalies to the average rain rate from the rain-gauge measurements (Table 2). The estimated lifetime is 11 hr. This lifetime can be interpreted as the characteristic time it takes for mixing to destroy a salinity anomaly. The estimated lifetime is crude because it is strongly influenced by large events on Day 116 and 117 and because the mixing rate depends on meteorological forcing which is highly variable. The characteristic lifetime from the data through Day 115 is 10 hr, insignificantly different from the estimate for the entire transect along the equator.

Newly-formed anomalies

Three large, newly-formed anomalies were selected for a detailed analysis. These anomalies will be used to compute rainfall temperatures. To ensure that the anomalies were newly-formed and of sufficient duration and magnitude to obtain meaningful rainfall temperatures, the following criteria were applied: 1) the length of time taken to traverse the anomaly exceeded 35 min (approximately 5.9 km), 2) the maximum salinity reduction within the anomaly relative to the smooth curve exceeded 0.6 PSU, 3) the maximum reduction of the temperature at 0.5 m relative to 5-m depth exceeded 0.1 C, and the temperature reduction at 1 m exceeded 0.03 C everywhere within the anomaly. The requirement for decreasing temperature with increasing elevation from the 5-m depth insures that an anomaly is sufficiently new not to have been well-mixed in the upper 5 m. The sign of the vertical temperature gradient caused by cold tropical rain is opposite to that caused by solar insolation. As further indication that the selected anomalies were newly-formed, rain was observed simultaneous or nearly simultaneous to the anomalies.

Meteorological conditions above and in the vicinity of the anomalies and the structure of the anomalies themselves are shown in Figs. 9, 10 and 11. Common to the three anomalies was a peak in the wind speed of 8 to 10 m/s nearly simultaneous to a drop in air temperature of about 3 C. A similar drop in air temperature was observed in squalls during the Global Atmospheric Research Program's Atlantic Tropical Experiment (GATE) by Barnes and Garstang (1982). The peak in wind was probably due to a gust front associated with a cool downdraft (Cotton and Anthes, 1989).

Fig. 9. The anomaly on Day 105 showing time/space series of 60-s wind speed, 30-min wind direction and 30-s air temperature, density, temperature, and salinity data for the anomaly on Day 105. The depths corresponding to different lines are defined in Fig. 2 (*e.g.* 0.5 m (thin line), 1 m (dashed line), 5 m (thick line)). The arrows mark the start and stop times of the 30-s, 1-m temperature and salinity data used to compute the rainfall temperature.

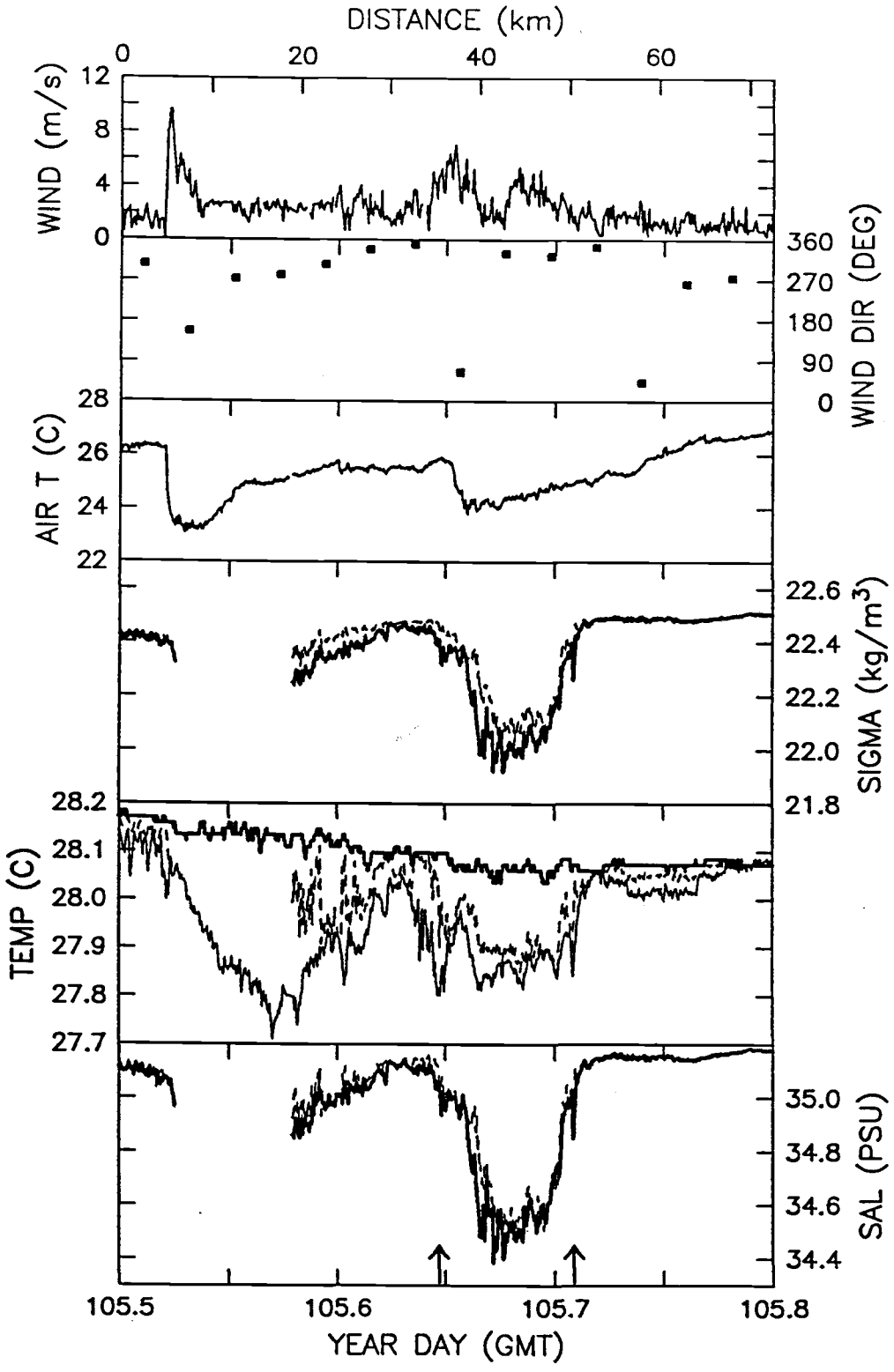
DISTANCE (km)
0
20
40
60
WIND (m/s)
12
8
4
0
WIND DIR (DEG)
360
270
180
90
0
AIR T (C)
28
26
24
22
SIGMA (kg/m3)
22.6
22.4
22.2
22.0
21.8
TEMP (C)
28.2
28.1
28.0
27.9
27.8
27.7
SAL (PSU)
35.0
34.8
34.6
34.4
105.5
105.6
105.7
105.8
YEAR DAY (GMT)

Fig. 9.

Fig. 10. Anomaly on Day 110, see caption Fig. 9. The vertical line marks the stop/start time which was used to split up the 1-m temperature and salinity data.

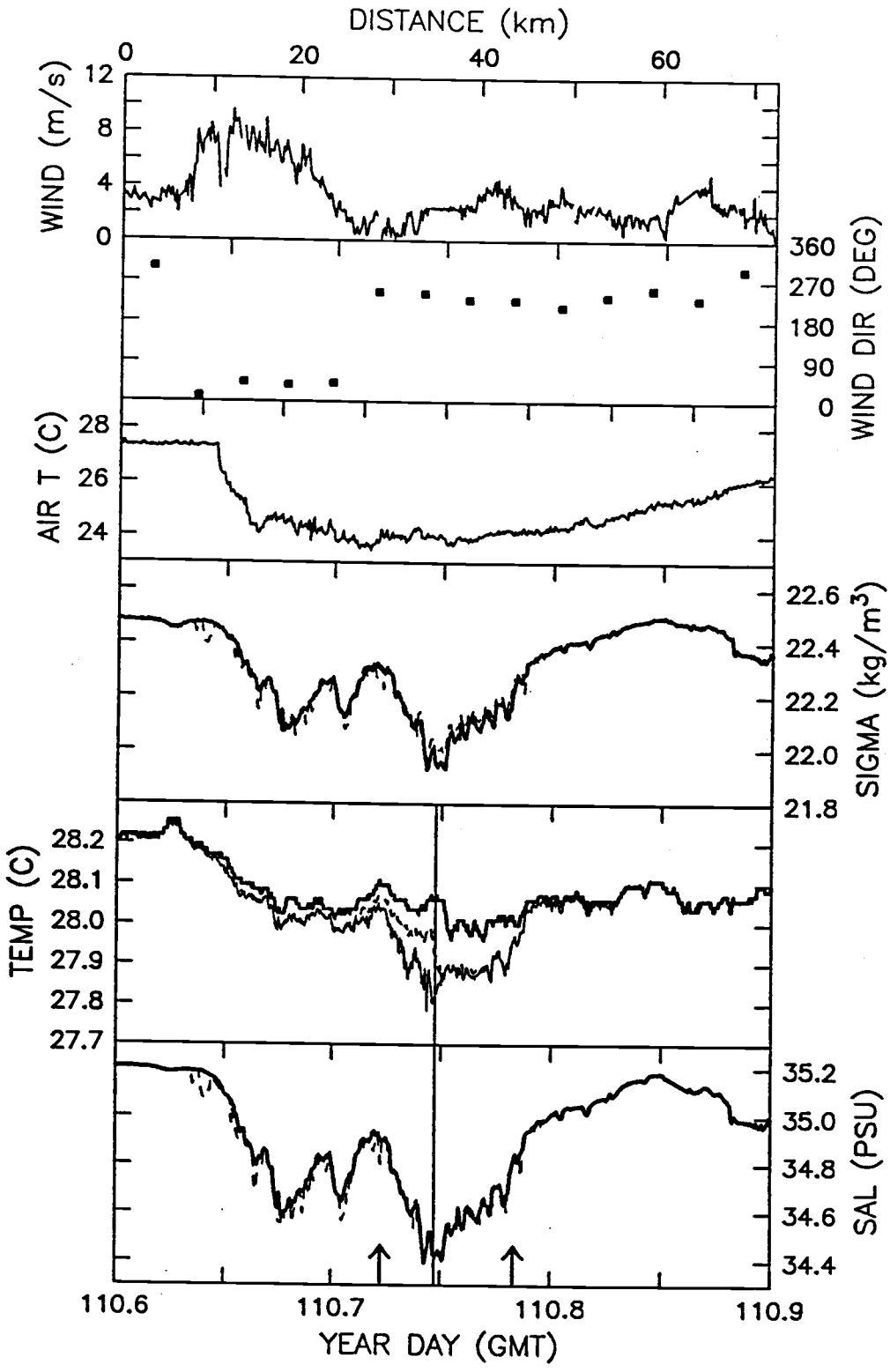
DISTANCE (km)
0
20
40
60
WIND (m/s)
12
8
4
0
360
270
180
90
0
WIND DIR (DEG)
AIR T (C)
28
26
24
22.6
22.4
22.2
22.0
21.8
SIGMA (kg/m3)
TEMP (C)
28.2
28.1
28.0
27.9
27.8
27.7
35.2
35.0
34.8
34.6
34.4
SAL (PSU)
110.6
110.7
110.8
110.9
YEAR DAY (GMT)

Fig. 10.

Fig. 11. Anomaly on Day 117, see caption Fig. 9.

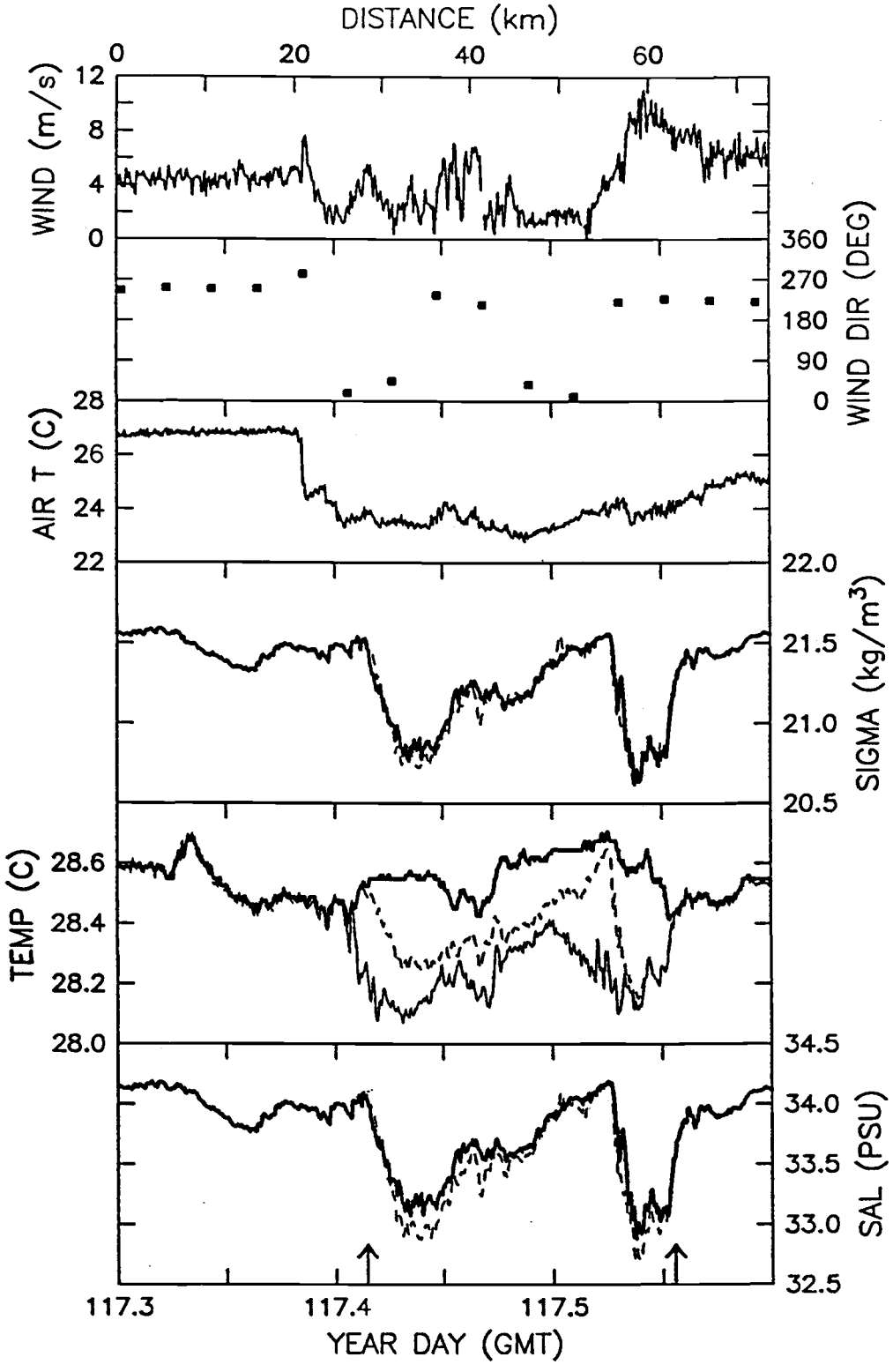
DISTANCE (km)
0
20
40
60
WIND (m/s)
12
8
4
0
WIND DIR (DEG)
360
270
180
90
0
AIR T (C)
28
26
24
22
SIGMA (kg/m3)
22.0
21.5
21.0
20.5
TEMP (C)
28.6
28.4
28.2
28.0
SAL (PSU)
34.5
34.0
33.5
33.0
32.5
117.3
117.4
117.5
YEAR DAY (GMT)

Fig. 11.

The beginning of heavy rain was probably associated with the drop in air temperature (Cotton and Anthes, 1989).

Temperature and salinity within the anomalies exhibit a high degree of variability and, on Days 105 and 117, a curious asymmetry (Figs. 9 and 11). The 5-m salinity is depressed nearly as much as the 1-m measurement, but there is no discernable temperature anomaly at 5-m depth. If the rain and its heat mix similarly, one would expect similar vertical structure in temperature and salinity. As yet, we have no explanation for the lack of similarity.

A schematic diagram of a rain storm and the resulting oceanic anomaly is shown in Fig. 12. The sketched oceanic anomaly of temperature and salinity is what one would expect if heat and water mixed similarly. As stated above, our observations are strikingly different.

Rainfall temperatures were estimated from the three newly-formed anomalies. Temperatures of the rain were estimated from mixing curves on temperature-salinity (T-S) diagrams. On a T-S diagram, two water types mix along a straight line joining them. Because rain water is fresh, one expects that extrapolation of a rain-caused mixing line to zero salinity will yield an estimate of the rainfall temperature. The method assumes that only mixing changes the temperature and salinity of the anomaly, which may be increasingly in error as time proceeds, because of possible modification due to air-sea exchanges. Figures 13, 14 and 15 show the T-S diagrams for the 1-m data between the arrows shown in Figs. 9, 10 and 11. Least squares linear fits to the data are also shown. The rainfall temperature estimates from the fits are presented in Table 3. The 80% confidence intervals were computed following Bendat and Piersol (1986, Eq. 4.75, page 104).

Fig. 12. Conceptual representation of a rain squall with idealized traces of the wind speed, air temperature, temperature, and salinity. The air flow arrows are drawn relative to the motion of the squall. The gray shading represents rainfall, the more intense the darker the gray.

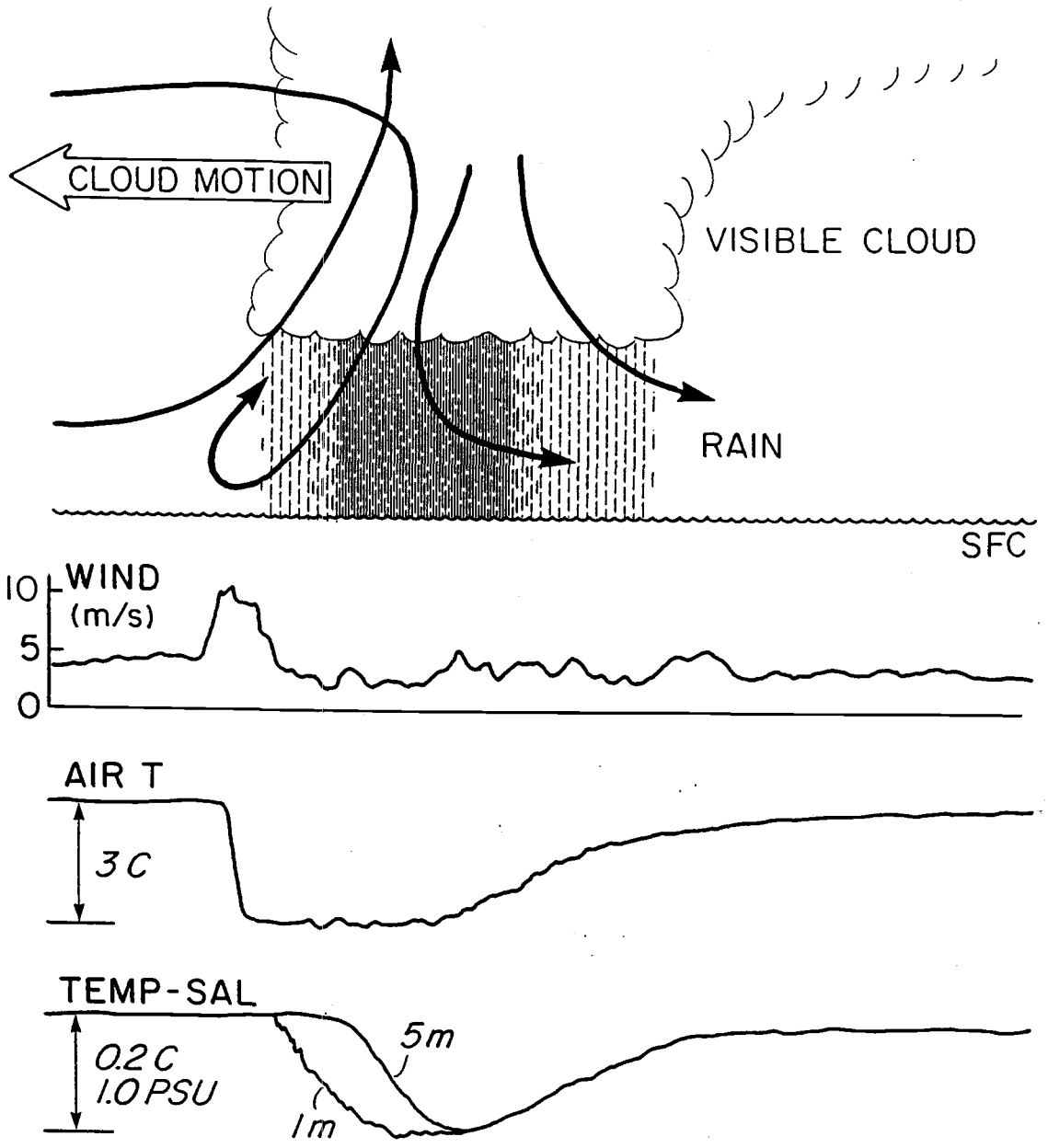
CLOUD MOTION
VISIBLE CLOUD
RAIN
SFC
10
WIND
(m/s)
5
0
AIR T
3C
TEMP-SAL
0.2C
1.0PSU
5m
1m

Fig. 12.

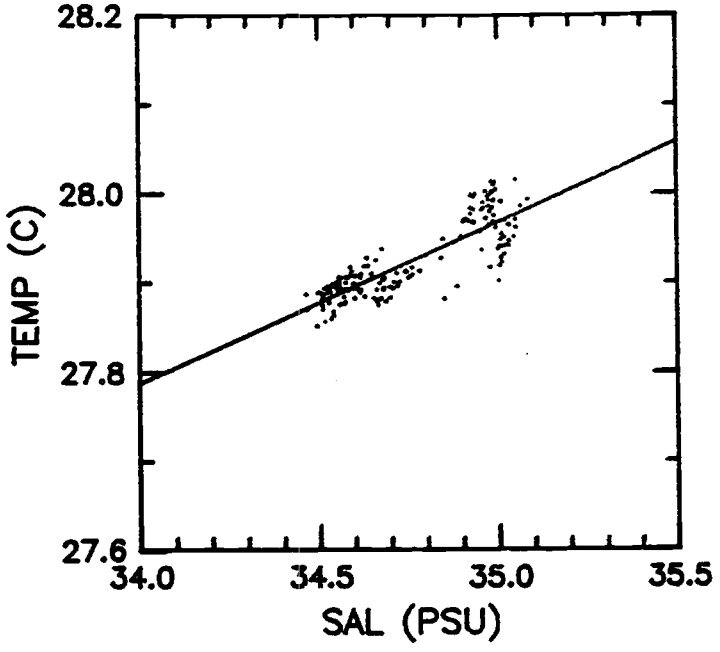

Fig. 13. T-S diagram of the 1-m data from the anomaly on Day 105. The least squares linear fit is T = 21.6+0.18S, where 21.6 is the estimated rainfall temperature by extrapolation of the line to zero salinity.

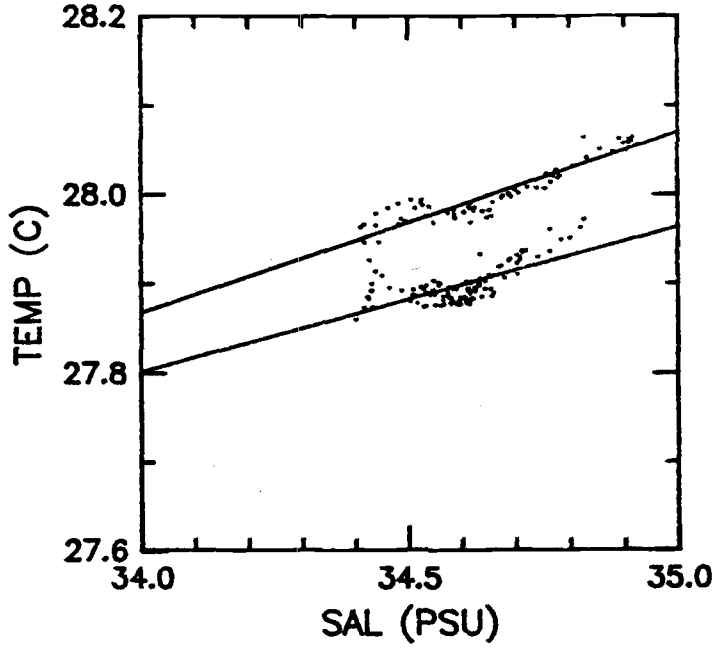

Fig. 14. T-S diagram of the 1-m data from the anomaly on Day 110. The least squares linear fits are T = 20.9 + 0.21S and T = 22.2 + 0.16S, where 20.9 and 22.2 are the rainfall temperature estimates.

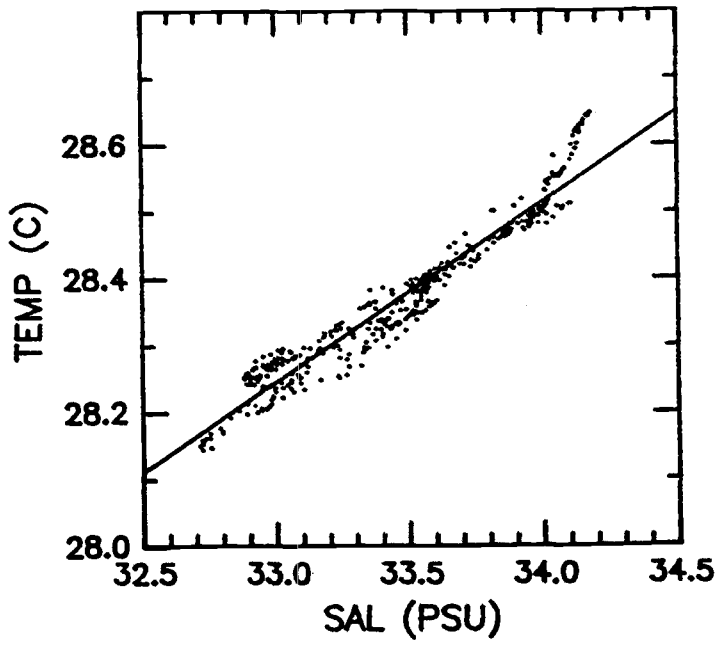

Fig. 15. T-S diagram of the 1-m data from the anomaly on Day 117. The least squares linear fit is $T = 19.3 + 0.27S$, where 19.3 is the rainfall temperature estimate.

Table 3. Characteristics of selected rainfall anomalies including start time, duration (Δt), vertical temperature gradient (ΔT), salinity anomaly (ΔS), rainfall temperature (Rain T) and 80% confidence interval of rainfall temperatures. All anomalies were selected which met the following criteria: $\Delta t > 35$ minutes, ΔS < -0.6 PSU and ΔT < -0.1 C. ΔS is the minimum difference (maximum absolute difference) between the smoothed background salinity and the 1-m salinity and ΔT is the minimum difference (maximum absolute difference) between the 0.5-m temperature and the 5-m temperature. The 80% confidence intervals for the individual estimates were computed following Bendat and Piersol (1986, Eq. 4.75, page 104). The 80% confidence interval for the average rainfall temperature was computed following Bendat and Piersol (1986, Eq. 4.46, page 86).

Start time (Year Day)	Δt (hrs)	ΔT (C)	ΔS (PSU)	Rain T (C)	Conf. (C)
105.6472	1.492	−0.21	−0.64	21.6	0.9
110.7226	0.583	−0.14	−0.72	20.9	1.0
110.7472	0.867	−0.20	−0.72	22.2	1.5
117.4146	3.383	−0.44	−1.59	19.3	0.7
Average:				21.0	
80% Confidence:				1.5	

The number of degrees of freedom was determined using the lag at which the lagged autocorrelation for the data fell to 50%. The confidence interval for the average of the four computed rain temperatures was computed following Bendat and Piersol (1986, Eq. 4.46, page 86). There is good agreement between the different confidence estimates.

Since the method assumes only mixing changes the temperature, other processes which change the temperature will be sources of error. Processes which change the salinity have also been ignored, since over the time scale involved (a few hours), evaporation would change the salinity by less than 0.02 PSU. The principle processes neglected are solar heating and the surface heat flux. The surface heat flux is relatively small over the longest period of 3 hrs. Solar heating, on the other hand, could cause the rainfall temperature estimates to be off by several degrees C. The effect of solar heating would have been to warm and/or tilt the mixing curve. The observations used to compute the rainfall temperatures were at night and in the early morning. Hence, we expect minimal errors due to air-sea exchanges.

Rain falling through a homogeneous layer will eventually reach an equilibrium temperature equal to the wet-bulb temperature of the layer (Kinzer and Gunn, 1951). The estimated average rainfall temperature is significantly less than the average surface wet-bulb temperature (21.0 C compared to 24.7 C, Tables 2 and 3). However, the minimum wet-bulb temperature (22.6 C) is substantially closer and may be more representative of surface values during rain squalls. One also expects rain to fall through air with increasing wet-bulb temperature and the drop may therefore depart from equilibrium and be colder than the wet-bulb temperature at the surface. Kinzer and Gunn (1951) found that drops 2.7 mm in diameter have a ther-

mal relaxation time of 4.35 s. For a step change in temperature, a drop of this size at terminal velocity would travel 20 m before reaching equilibrium.

Evolution of T-S anomalies

In the absence of wind and waves, energy from the initial mixing of rainfall with the upper ocean will come only from the kinetic energy of the drops themselves. Katsaros and Buettner (1969) and Green and Houk (1979) have investigated rain-induced mixing in the laboratory and observed mixing depths as large as 30 cm, with large drops being the most effective.

Following the initial mixing by the kinetic energy of rain drops, wind forcing would continue to deepen the anomaly. The time scale for this mixing can be estimated from simple turbulence theory as $-z/u^*$, where $-z$ is the depth and u^* is the friction velocity ($(\tau/\rho)^{1/2}$, where τ is wind stress and ρ is water density). Typical values of u^* are 0.01 m/s. For a depth of 5 m, the time scale would be 500 s. This time can be interpreted as the time-scale for a turbulent eddy within an unstratified turbulent boundary layer. The effect of stable salt stratification would be to retard the mixing rate.

The lenses of low density water will tend to spread due to pressure gradient forces. Garvine (1974) has investigated this phenomena. Because the data were taken on the equator, the Coriolis force is 0, and the speed of the propagation of the front (rate of spreading) is given by the phase velocity of the first internal wave mode

$$U_{\mathbf{front}} = (g D_{\mathrm{d}} \Delta\rho/\rho)^{1/2}$$

where g is the acceleration due to gravity, ρ is the density of the surrounding fluid, $\Delta\rho$ is the density difference between the fresh lens and the surrounding fluid, and D_{d} is the maximum depth of the fresh lens (Garvine, 1974). The rate of spreading is given relative to the background water. Using values from Table 2, we obtain a speed of 6 cm/s.

The rain-formed lenses may also be advected by the wind. The mean surface velocity driven by the wind is approximately 3% of the wind speed, which for the average winds observed along the zonal transect is 10 cm/s, comparable to the rate of spreading due to the pressure gradient. One would expect the wind-driven surface velocity to decrease rapidly with depth under the influence of stable stratification. One might expect that at the upwind edge of the lens, there would be advection of dense surrounding surface water into the lens and result in convectively-driven mixing and sharpening of the front. The observations were examined for such an effect, but it was not found. The effect might be difficult to discern because of the high degree of variability within the anomalies.

Effects of rainfall on air-sea fluxes

Rainfall may contribute substantially to air-sea exchanges of water and heat. Estimates are given in Table 2. The average rain rate over the duration of the transect was a factor of seven greater than the average evaporation rate. The estimated average rain depth over the transect is substantially influenced by the large salinity anomalies on Days 116 and 117, and the mean rain rate is strongly influenced by the maximum rain-gauge measurement on Day 117. Values of rain-influenced parameters were also computed only through Day 115 and are also shown in Table 2. With Days 116 and 117 excluded, average rainfall exceeds average evaporation by a factor of four.

Because the rainfall was colder than the sea surface temperature, there was a positive (upward) heat flux associated with the rain. The heat flux due to rain is

$$H_{\mathbf{rain}} = (T_{\mathbf{s}} - T_{\mathbf{r}})\ \rho\ R\ C_p$$

where $T_{\mathbf{s}}$ is sea surface temperature, $T_{\mathbf{r}}$ is the rain temperature, C_p is the heat capacity of the rain water, ρ is the density of rain water, and R is the rain rate. On average, the heat flux associated with the rain was only 6% of the total heat flux. When Days 116 and 117 are excluded, the contribution associated with rain drops to 3%. However, the maximum heat flux associated with intense rainfall was comparable to the average total excepting rain.

The buoyancy flux due to rain is given by

$$J_{\mathbf{rain}} = \Delta\rho/\rho\ R$$

where $\Delta\rho$ is the difference in densities between the rain and the sea water, ρ is the density of the rain, and R is the rain rate. The average contribution of

rain to the oceanic buoyancy flux was 40% of the total buoyancy flux due to all processes except solar insolation. When Days 116 and 117 are excluded, the contribution by rain drops to 20%. Maximum contributions of rain to the buoyancy flux are about an order of magnitude greater than the mean contributions.

Another effect of rainfall is the trapping of heat in a thin surface layer because of salt-stratification. Stable stratification will inhibit vertical mixing and because there is net heating of the surface, surface temperatures will be increased. Diurnal peaks of surface temperature associated with solar insolation would also be enhanced. We have not been able to extract such signals from the observations, but they have been reported by Ginzburg *et.al.* (1980) and Volkov *et. al.* (1989).

Conclusion

Observations in the upper 5 m along the equator in the eastern equatorial Pacific during April and May, 1987, an *El Niño* year, show low-salinity, low-temperature anomalies caused by rain. The anomalies ranged in horizontal extent from less than 10 to more than 100 km and there was a rough linear relationship between the magnitude of a salinity anomaly and its horizontal scale (Fig. 7). The maximum salinity anomaly at 1-m depth was 1.6 PSU (departure of the 30-s sample from the smooth background). The maximum rain-caused temperature anomaly was a cooling at 0.5 m of 0.5 C relative to the temperature at 5-m depth (coldest at 0.5 m).

Rainfall depth was estimated from conservation of salt, yielding a maximum depth of 14 cm. There was rough agreement between a local maximum rain depth of 14 cm with a near-simultaneous rain-gauge measurement of 11 cm over 15 hr. The characteristic lifetime of the anomalies, estimated from the ratio of average rain depth to average rain rate was about 10 hours.

The average rainfall temperature, estimated by extrapolating T-S mixing lines to zero salinity, was 21.0 C (Table 3), significantly colder than the mean wet bulb temperature but not significantly different at the 80% confidence level than the minimum wet-bulb temperature (Table 2).

The effect of rain on air-sea exchanges was assessed. The effect of rain on heat flux was, on average, only 3 to 6%, but during periods of heavy rain, the effect can be comparable to the mean. The contribution of rain to buoyancy flux (neglecting solar radiation) was 20 to 40% on average. During periods of heavy rainfall the contribution by rain can dominate.

Bibliography

Barnes, G.M. and M. Garstang, 1982: Subcloud layer energetics of precipitating convection. *Mon. Wea. Rev.*, **110**, 102–117.

Bendat, J.S. and A.G. Piersol, 1986: *Random Data Analysis and Measurement Procedures.* John Wiley and Sons, Inc., 566 pp.

Cotton, W.R. and R.A. Anthes, 1989: *Storm and Cloud Dynamics.* Academic Press, Inc., 883 pp.

Esbensen, S.K. and Y. Kushnir, 1981: The heat budget of the global ocean: An atlas based on estimates from surface marine observations. Climate Research Institute Rept. #29, Oregon State University, 27 pp. + figs.

Garvine, R.W., 1974: Dynamics of small-scale oceanic fronts. *J. Phys. Oceanogr.*, **4**, 557–569.

Ginzburg, A.I., A.G. Zatsepin, V.Ye. Sklyarov and K.N. Fedorov, 1980: Precipitation effects in the near-surface layer of the ocean. *Oceanology*, **20**, 544–549.

Green, T. and D.F. Houk, 1979: The mixing of rain with near-surface water. *J. Fluid Mech.* **90**, 569–588.

Hebert, D., J.N. Moum, C.A. Paulson, D.R. Caldwell, T.K. Chereskin and M.J. McPhaden, 1991: The role of the turbulent stress divergence in the equatorial Pacific zonal momentum balance. *J. Geophys. Res.*, **96**, 7127–7136.

Katsaros, K. and K.J.K. Buettner, 1969: Influence of rainfall on temperature and salinity of the ocean surface. *J. Appl. Meteor.* **8**, 15–18.

Kinzer, G.D. and R. Gunn, 1951: The evaporation, temperature and thermal relaxation-time of freely falling water drops. *J. Meteor.*, **8**, 71–83.

Large, W.G. and S. Pond, 1981: Open ocean momentum flux measurements in moderate to strong winds. *J. Phys. Oceanogr.*, **11**, 324–336.

Large, W.G. and S. Pond, 1982: Sensible and latent heat flux measurements over the ocean. *J. Phys. Oceanogr.*, **12**, 464–482.

Levitus, S., 1982: Climatological atlas of the world ocean. National Oceanic and Atmospheric Administration Professional Paper No. 13, Rockville, Md., 173 pp.

Lukas, R., 1990: Freshwater input to the western equatorial Pacific Ocean an air-sea interaction. Proceedings of the Symposium on Western Tropical Pacific Air-Sea Interactions, Beijing, 15–17 Nov. 1988.

Ostapoff, F., Y. Tarbeyev and S. Worthem, 1973: Heat flux and precipitation estimates from oceanographic observations. *Science*, **180**, 960–962.

Philander, S.G.H., 1990: *El Nino, la Nina, and the Southern Oscillation.* Academic Press, 293 pp.

Pickard, G.L. and W.J. Emery, 1982: *Descriptive Physical Oceanongraphy An Introduction.* Pergamon Press, 249 pp.

Price, J.F., 1979: Observations of a rain-formed mixed layer. *J. Phys. Oceangr.*, **9**, 643–649.

Taylor, R.C., 1973: An atlas of Pacific islands rainfall. Hawaii Inst. Geophys. Data Rept. 25, HIG-73-9.

Volkov, Yu.A., A.V. Solov'yev, V.V. Turenko, V.A. Bezverkhniy, N.V. Vershinskiy and F.M.A. Yermolayev, 1989: Measurements of the structure for the Hydrophysical fields of a thin ocean surface layer from a moving ship. *Izv. Acad. Sci. USSR, Atmos. Ocean. Phys.*, **27**, 512–516.

Weare, B.C., P.T. Strub and M.D. Samuel, 1981: Annual mean surface heat fluxes in the tropical Pacific Ocean. *J. Phys. Oceangr.*, **11**, 705–717.